Fabrication of an UltraLow-Resistance Ohmic Contact to MWCNT–Metal Interconnect Using Graphitic Carbon by Electron Beam-Induced Deposition (EBID)

Songkil Kim, Dhaval D. Kulkarni, Konrad Rykaczewski, Mathias Henry, Vladimir V. Tsukruk, and Andrei G. Fedorov

***Abstract*—Reduction in contact resistance is one of the foremost challenges for carbon nanotube/graphene nanodevices. In this study, we present a novel fabrication process for low-temperature, Ohmic contact between open-ended multiwalled carbon nanotubes (MWCNTs) and metal interconnects using graphitic carbon deposited via electron beam-induced deposition (EBID). The electrical and structural properties of the contact interface are characterized for making connection to the single (outermost) shell only, as well as to multiple conducting shells of MWCNTs. In addition to establishing the scaling relationship between the carbon contact length and the resulting contact resistance, the magnitude of the contact resistance has been quantified with and without post-deposition thermal annealing. The results indicate that the contact is Ohmic in nature, and ranges from 26.5 kΩ for the connection made to the outermost shell of an MWCNT down to just 116 Ω for the multiple-shell connection performed via a process suggested through the EBID process simulations. These results provide a significant advance in application of MWCNTs to future interconnect technologies.**

***Index Terms*—Contact resistances, electron beam-induced deposition (EBID), multiwalled carbon nanotube (MWCNT), MWCNT–metal interconnect.**

I. Introduction

CARBON nanotubes (CNTs) are promising candidates for the replacement of copper-based interconnects in electronic devices [1]. However, one of the main challenges for the interconnect application of CNTs is the high contact resistance to the metal electrodes [2]. Recently, significant progress has been made in assessing the resistance of metal contacts to single-walled CNTs (SWCNTs) [3], [4]. It was found that the contact resistance to a metallic SWCNT can be reduced down to the quantum limit (∼6.5 kΩ) with the channel length scaled down to 15 nm [3]. Even with this notable achievement, there are still a number of competing factors that need to be considered and technical challenges to be overcome in order to achieve the superior electrical performance promised by the CNTs [1].

One of the alternatives is to utilize a multiwalled CNT (MWCNT) and to make connection to multiple conducting shells, acting as parallel conducting channels. However, it is fundamentally challenging to connect multiple conducting shells of an MWCNT using standard metal deposition processes due to the limited control of directionality (in three dimensions) in a standard contact fabrication process using nanolithography followed by metal evaporation/sputtering [6], [7]. Also, metal deposition using sputtering or evaporation only yields a physical contact to the MWCNT, which results in a week electronic coupling at the Fermi surface [2], [8]. Theoretical calculations revealed that the contact resistance between metal and the open end of a carbon nanotube is on the order of 3–4 kΩ even for contamination-free contact interface [9], [10]. Alternative fabrication methods have been demonstrated for establishing chemical binding of multiple CNT shells to metal [6], [7], [11]. For example, a TEM–AFM combination with the piezomotor-driven nanomanipulator was utilized to precisely position the open end of an MWCNT in contact with a tungsten AFM tip; then, the MWCNT and the tip were fused by Joule heating to establish a multiple shell contact to the metal. Such an MWCNT–carbide–metal interface resulted in very low Ohmic contact resistance of 700 Ω [11]. Obviously, while yielding a high-quality electrical contact, this technique is not amenable for the scalable fabrication of electronic devices and the contact area/geometry between an MWCNT and a metal tip is limited to whatever spontaneously forms in the course of an intense heat release at the contact junction with a rather poor control over the final outcome.

On the contrary, electron beam-induced deposition (EBID) is a technique in which a focused electron beam facilitates a chemical vapor deposition (CVD) process with high degree of spatial and time-domain control [12], [13]. It has three main advantages for fabricating a contact interface between the MWCNT and a metal interconnect. First, it allows the use of a variety of materials for forming a contact junction [14]. Of particular interest here is carbon deposition using readily available hydrocarbon precursors. Carbon is superior as an interfacial material in that

Manuscript received June 8, 2012; accepted September 11, 2012. Date of publication October 4, 2012; date of current version November 16, 2012. This work was supported in part by the Semiconductor Research Corporation under Contract 2008OJ1864.1281 and in part by the National Science Foundation under Grant DMI 0403671. The review of this paper was arranged by Associate Editor L. Dong.

S. Kim, M. Henry, and A. G. Fedorov are with the Woodruff School of Mechanical Engineering, Georgia Institute of Technology, Atlanta, GA 30332-0405 USA (e-mail: andrei.fedorov@me.gatech.edu).

D. D. Kulkarni and V. V. Tsukruk are with the School of Materials Science and Engineering, Georgia Institute of Technology, Atlanta, GA 30332-0405 USA.

K. Rykaczewski is with the Department of Mechanical Engineering, Massachusetts Institute of Technology, Cambridge, MA 02139 USA.

Color versions of one or more of the figures in this paper are available online at http://ieeexplore.ieee.org.

Digital Object Identifier 10.1109/TNANO.2012.2220377

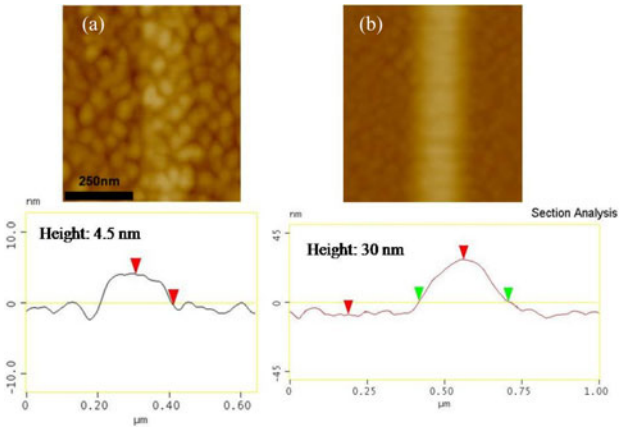

Fig. 1. AFM images and cross-sectional profiles for EBID-made carbon line on a copper substrate with deposition time of (a) 30 s and (b) 5 min, showing an excellent wettability of the carbon–Cu pair.

an intrinsic resistance of the contact to the MWCNT can be made negligibly small since carbon has good wettability to both a CNT and most metals. Fig. 1 shows an AFM image and cross-sectional profile of a thin EBID-made carbon line on a copper substrate. It shows a smooth and continuous interface between the copper substrate and the carbon deposit indicative of an excellent wettability. Additionally, the CNT–carbon–metal junction should have an Ohmic behavior due to similarity of work functions for all the three materials [15]–[17]. Second, deposition of the contact material is precisely controlled (both the rate of growth and the resulting 3-D shape) by simply changing the electron beam current and accelerating voltage [12], [18], [19] and moving the sample stage so that the deposit's access to multiple shells can be achieved. Finally, this technique can be applied to scalable fabrication of actual multi-interconnect devices by using a multibeam system [20] in conjunction with controllable alignment of MWCNTs on prefabricated electrodes. Our previous work established the potential of EBID carbon joint to MWCNT–metal interconnect to improve the contact resistance [12]. However, there is still a significant room to improve the EBID contact fabrication process including making a connection to multiple shells of MWCNTs [13], lowering the contact resistance close to the order of the MWCNT channel resistance through preferential phase transformation of the carbon contact, and a controllable MWCNT assembly in parallel (i.e., multielectrode) format.

To this end, in this study we aim to accomplish several objectives: 1) to fabricate EBID carbon contacts to the outermost shell of an MWCNT in order to understand the geometric effects on the contact resistances and to develop the contact size-dependent scaling laws; 2) to critically evaluate and optimize the EBID deposit annealing technique to improve conductivity of the carbon contacts; and 3) most importantly, experimentally demonstrate a new fabrication protocol, which is suggested based on comprehensive simulations, for making connection to multiple shells of the MWCNTs, which yields an ultralow-resistance Ohmic contact between a MWCNT and metal electrodes. These EBID and post-deposition advances are supplemented with innovations in other enabling processing steps, such as a controlled assembly/alignment of multiple MWCNTs onto an array of metal electrodes.

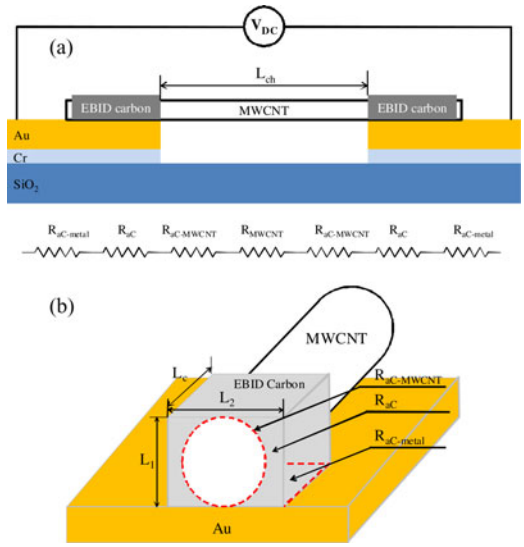

Fig. 2. Schematics of (a) device structure and the experimental setup for two-point electrical measurements, and (b) geometry of an EBID carbon contact and contributing resistances to the overall contact resistance.

II. Results and Discussions

A. Scaling of EBID-Made Carbon Contact to the Outermost Shell of a MWCNT

First, we investigated a geometry and size effect of EBID carbon joints on the magnitude of the contact resistance. In two-point measurements using a setup schematically shown in Fig. 2(a), the total resistance of an MWCNT–metal interconnect with EBID carbon joints can be expressed as [12],

$$R_{\rm tot} \approx 2R_{\rm aC} + 2R_{\rm aC-metal} + 2R_{\rm aC-MWCNT} + R_{\rm MWCNT}. \quad (1)$$

As found in our previous work, the dominant factor in the total interconnect resistance is the resistance of the EBID carbon joint, whereas the interface resistance between the EBID carbon joints and an MWCNT does not have a significant influence on total resistance [12]. The components of total resistance in (1) can be expressed in terms of relevant dimensions and intrinsic electrical conductivities of the materials

$$R_{\rm tot} \approx \frac{2}{L_c}\left(\frac{\rho_{\rm aC}L_1}{L_2} + \frac{\sigma_{\rm aC-metal}}{L_2} + \frac{\sigma_{\rm aC-MWCNT}}{\pi d_{\rm MWCNT}}\right) + R_{\rm MWCNT}. \quad (2)$$

Here, $\rho_{\rm aC}$ is the resistivity (Ω·m) of the amorphous EBID carbon as deposited, $\sigma_{\rm aC-metal}$ is an interfacial area resistivity (Ω·m^2) between the carbon contact and the metal electrode, $\sigma_{\rm aC-MWCNT}$ is an interfacial area resistivity (Ω·m^2) between the carbon contact and an outermost shell of a MWCNT, and all the dimensions are described in Fig. 2(b). Equation (2) indicates that an interconnect resistance is inversely proportional to a contact length L_c of carbon interface to an MWCNT, and asymptotically approaches to the intrinsic resistance of an MWCNT itself in the limit of an ideal contact. The resistance of defect-free MWCNTs can be evaluated by (3) for an outermost shell

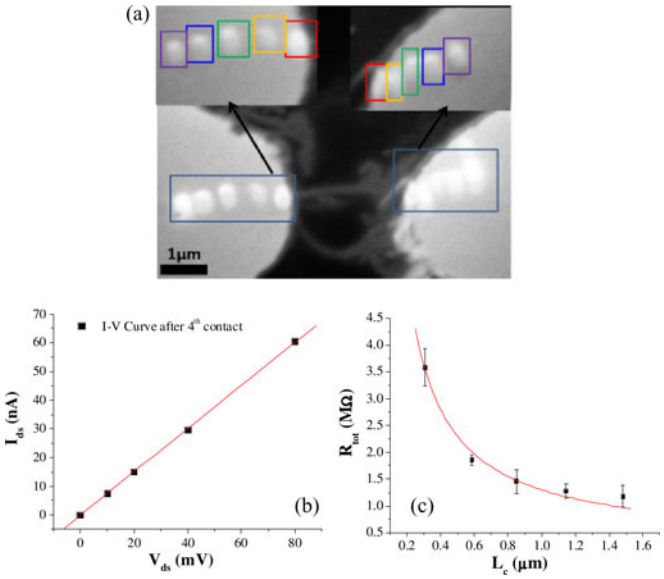

Fig. 3. (a) Series of EBID-made carbon contacts to the outer shell of MWCNT ($D_{\rm cnt}\sim$30 nm). (b) $I-V$ curve after fourth contact-pair fabrication showing linear Ohmic behavior. (c) Overall interconnect resistance $R_{\rm tot}$ measurement with increasing contact length L_c by sequential pairwise deposition of carbon squares on both ends of an MWCNT demonstrates $R_{\rm tot}\sim P_1/L_c+P_2$ and suggests a need to decrease the intrinsic resistivity P_1 of the contacts by graphitization of EBID carbon, along with minimizing the channel resistance of an MWCNT P_2.

contact only [3], [10]

$$R_{\rm MWCNT}=\frac{h}{2\bar{N}e^2}\left(1+\frac{L_{\rm ch}}{L_{\rm mfp}}\right) \tag{3}$$

where $h/2e^2\sim$12.9 kΩ, $\bar{N}$ is the average number of conducting channels in one shell [10], $L_{\rm ch}$ is a channel length of an MWCNT, and $L_{\rm mfp}$ is the mean free path of an electron approximated to be about a factor of a thousand of the CNT diameter [10], [12], [21].

To verify the validity of the (2) scaling law, a series of rectangular carbon deposits were fabricated atop of the outermost shell of a MWCNT with a diameter of ∼30 nm, as shown in Fig. 3(a) (see Appendix A for deposition parameters). The resistance of an ideal MWCNT with an outermost shell contact is estimated using (3) to be ∼3.75 kΩ for the channel length of 2 μm. Upon a series of pairwise depositions of contacts on both ends, the $I-V$ measurements for the resulting interconnect were performed for the 0–80 mV voltage range. All $I-V$ curves were linear as shown in Fig. 3(b), indicating an Ohmic contact, which allows computation of the total interconnect resistance from the slope. A contact length for each deposit pair was defined as an average value for two contacts to metal electrodes on both ends. As shown in Fig. 3(c), the overall resistance is inversely proportional to the contact length L_c between carbon contacts and MWCNT with P_1 denoting the resistivity of contact interfaces and P_2 is an MWCNT channel resistance. By fitting the experimental data to this scaling law, the resistivity P_1 is found to be ∼1.0 Ω·m, which is much higher than that for metal contact (1 e−6 Ω·m) due to a low electrical conductivity of as-deposited hydrogenated, amorphous EBID carbon [3], [12], [22].

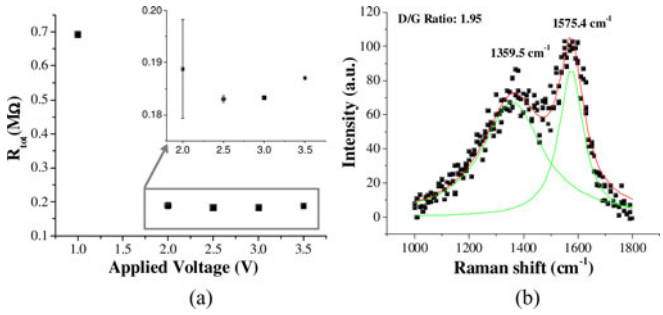

Fig. 4. (a) Joule-heating-induced annealing of the carbon contacts significantly reduces the overall interconnect resistance by graphitization of contacts. (b) Raman spectra of EBID carbon contacts after Joule-heating-induced annealing, which indicates the partially graphitized structure of the contacts.

B. Graphitization of EBID Carbon Contacts for Low Contact Resistances

To increase a conductivity of EBID carbon contacts, we graphitized the amorphous EBID carbon deposits using Joule-heating-induced annealing in vacuum by passing an electric current through an MWCNT interconnect with EBID-deposited contacts. As shown in Fig. 4(a), the contact resistance is reduced by an order of magnitude from 1.1 to 0.18 MΩ due to carbon graphitization. Increasing of the contact length to 1.8 μm and subsequent Joule heating at 1 V reduces the resistance to 130 kΩ. Further increase in the bias voltage beyond 2 V (i.e., higher annealing currents) to stimulate further annealing of the contacts yielded a negative result with the total resistance starting to increase to 230 kΩ, likely due to thermomechanical damage of the MWCNT upon excessive Joule heating [23], [24]. In order to understand the composition of the carbon deposits, Raman spectroscopy was utilized [see Fig. 4(b)]. The G-peak position and D/G ratio are 1575.4 cm^{-1} and 1.95, respectively, suggesting the partially graphitic nature of the EBID carbon deposits after annealing. The fully graphitized structure resulting from annealing of hydrogenated amorphous carbon is known as a nanocrystalline graphite, which has a G-peak position of around 1600 cm^{-1} and D/G ratio of around 2.5 [22]. This supports our observation that a damage of the MWCNT due to Joule heating is the most likely cause of an increase of the overall interconnect resistance before the EBID carbon contacts can be fully graphitized.

Annealing by Joule heating is rather difficult to control without inducing a parasitic thermomechanical damage, owing to the fact that the resistance of the carbon continuously decreases as it undergoes phase transformation, which results in a run-away increase in the current (and thus heat release) when the same electric potential bias is applied. As an alternative, which offers a significantly greater control, we performed thermal annealing in a controlled-environment furnace to avoid any physical damage of the tubes, yet to be able to fully graphitize the EBID carbon contacts. It is known that EBID nanosized carbon deposits start to graphitize at much lower (∼350 °C) than the bulk carbon phase-transition temperature, and formation of a highly densified graphitic deposit (nanocrystalline graphite) occurs at around 450 °C in an environment furnace [22]. Thus, to fully graphitize the EBID carbon contact, one needs to increase the annealing temperature to 450 °C, but the MWCNTs begin to

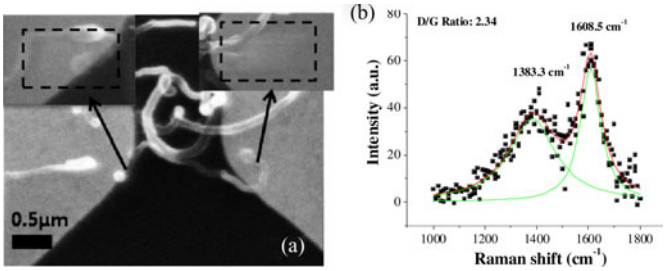

Fig. 5. (a) EBID-made carbon contacts (magnified in the insets) to an outermost shell of a larger diameter of an MWCNT ($D_{\rm cnt} \sim 75$ nm) yielding the overall resistance of 26.5 kΩ after thermal annealing at 350 °C for 30 min; and (b) Raman spectroscopy measurements indicating the carbon contacts are fully graphitized after the thermal annealing process at 350 °C for 30 min.

oxidize around this temperature [25]. To avoid the oxidation of MWCNT, we annealed the contacts at 350 °C in an environment furnace, which is a threshold temperature of graphitization of EBID carbon nanostructures. It is worth to note that there are two contributing factors in determining the carbon structure after an annealing process; a base substrate as a site for a nucleation of the graphitic crystallites and an interfacial area between the EBID carbon structure and the metal substrate [22]. The optimized annealing temperature in the literature was determined for carbon dot and line deposits on Au/Cr substrate [22]. The presence of MWCNTs beneath the EBID carbon structure can have an influence on lowering the graphitization threshold temperature and defining a preferred (CNT-like) phase that the carbon accepts upon annealing.

To minimize the influence of the MWCNT resistance on the overall interconnect resistance, we utilized a larger diameter MWCNT from a commercial vendor [26], which were fabricated by the arc discharge method. It has a diameter of 75 nm and the channel length of around 2 μm, as shown in Fig. 5(a), with its outermost shell resistance computed to be about 1.5 kΩ by (3) if it is defect free. We fabricated square-like carbon contacts on both ends of the tube [see the insets of Fig. 5(a)] to establish a contact between the outermost shell of the CNT and the metal electrodes. Initially (i.e., before contact deposition) when an isolated MWCNT was aligned between two metal electrodes, the overall interconnect resistance was ∼1 GΩ. After deposition of the EBID carbon contacts at the ends of the MWCNT, the resistance dropped significantly down to 13 MΩ. Thermal annealing at 350 °C for 30 min in an ambient environment furnace resulted in further reduction of the overall interconnect resistance to 26.5 kΩ. This indicates that the contact resistance is at least below 25 kΩ, which is the resistance after subtracting that of the ideal tube itself from the total measured resistance, and it is likely to be much lower due to intrinsic defects in the MWCNT and also because of the presence of kinks further reducing electrical conductance [27].

The carbon contact structure was evaluated using Raman spectroscopy. As shown in Fig. 5(b), the G-peak position and D/G ratio reveal that the contact has characteristics of a nanocrystalline graphite, suggesting that graphitization of the EBID carbon structure can be achieved at much lower annealing temperature in the presence of MWCNTs than in the case of the plain metal substrate [22]. It should be mentioned that all electrical measurements were performed with low-bias (0–80 mV) voltage to avoid accidental Joule-heating-induced damage of the tube.

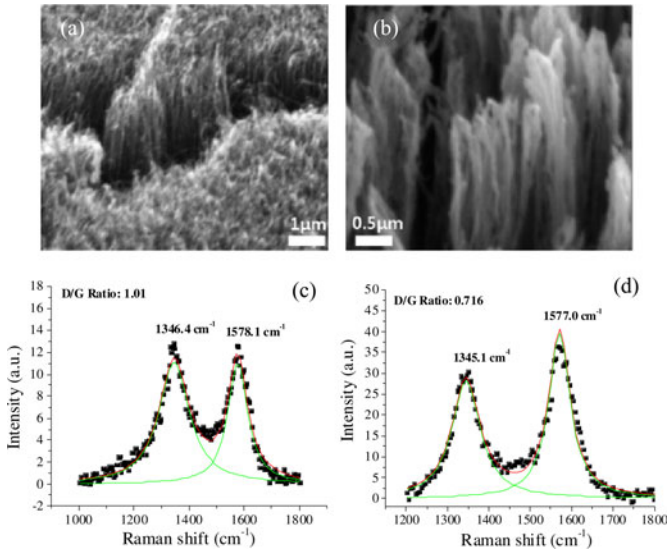

Fig. 6. SEM images of (a) as-grown CVD MWCNT forests and (b) after Ar plasma etching for 30 min. Raman measurements for (c) as-grown MWCNT forests and (d) after the plasma etching. It indicates that the quality of the forests slightly improved after the plasma treatment due to amorphous carbon layer removal.

C. Making EBID Contact to Multiple Shells of an MWCNT

1) Preparation of Open-Ended MWCNTs: A dense forest of MWCNTs with diameter ranging from 10 to 35 nm was grown using a conventional CVD on a silicon substrate, as shown in Fig. 6(a). Initially, capped ends of MWCNTs need to be opened up to expose all shells for making the contacts to metal electrodes. Thus, the forest of MWCNTs was subjected to an Argon plasma treatment in order to electrochemically etch away the end caps of MWCNTs [28]. After an exposure for 30 min, the length of the MWCNTs reduced from 18 to 10 μm which indicates successful plasma etch and opening the ends of MWCNTs exposed to the plasma. Interestingly, as shown in the Raman spectra for the MWCNT forests, Fig. 6(c) and (d), the quality of the tubes slightly improved after the plasma treatment due to a positive "side effect" of the amorphous carbon layer removal. The etched MWCNTs were subsequently released from the substrate by mechanical stripping and dispersed in Dimethylformamide (DMF) with assistance of ultrasonication. This process further breaks the MWCNTs along their lengths and results in a solution containing primarily open-ended MWCNTs of shorter length (< 8 μm).

2) EBID Modeling and Selection of the Deposition Process Parameters: Comprehensive simulations of EBID process have been used to propose and guide a fabrication protocol for making connection to the multiple shells of an MWCNT interconnect. We extended our previously developed model [29] in which an MWCNT is modeled as a carbon cylinder with a diameter of 30 nm coupled to the substrate as shown in Fig. 7(a). A typically used EBID spot mode, which forms the cone-shaped deposits in the precursor transport-limited deposition regime,

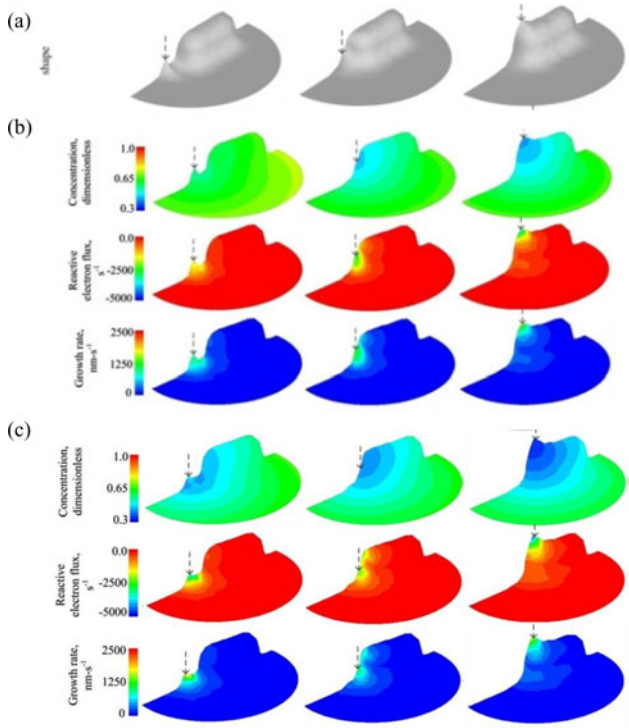

Fig. 7. (a) Simulation geometry with three different locations of electron beam impingement. Simulation results assessing the effect of the electron beam energy, (b) 10 keV, and (c) 25 keV, after 0.2-s deposition time indicate that the electron beam energy does not influence the shape and growth rate of deposits.

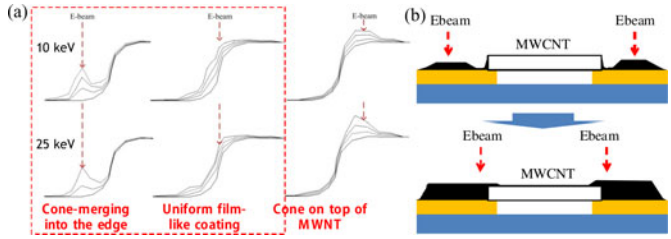

Fig. 8. (a) Cross sections of simulated EBID carbon deposits along the MWCNT axis for 10 keV (top) and 25 keV (bottom) beam energies, and (b) schematic of the optimal EBID contact fabrication protocol to connect the multiple shells of MWCNT as suggested by simulations.

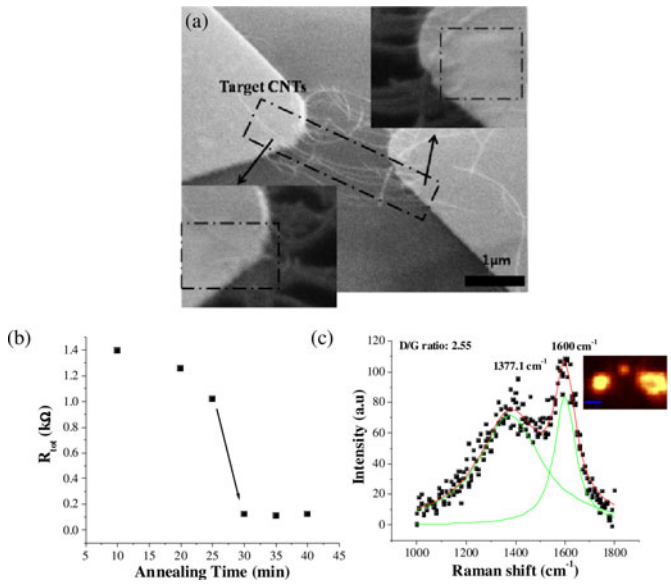

Fig. 9. (a) SEM image of an MWCNT interconnect and EBID carbon contacts connecting to the multiple inner shells of MWCNT. (b) Electrical performance measurements—the overall interconnect resistance reduced from 300 kΩ (as deposited) to 116 Ω after thermal annealing at 350 °C for 35 min in an ambient environment furnace and (c) Raman spectra of the EBID carbon, which indicate that the contacts become nanocrystalline graphite after annealing. The inset shows a Raman map of the EBID carbon contacts indicating that the deposits are fully graphitized.

was simulated for three different positions of an electron beam impingement relative to the end of an MWCNT, and using low (10 keV) and high (25 keV) electron beam energies to investigate the effect of the EBID conditions on the shape evolution of EBID carbon joint in the vicinity of open ends of the MWCNT.

Fig. 7(b) and (c) shows the effect of the electron beam energy on the deposit shape, hydrocarbon precursor surface concentrations, secondary "reactive" electron flux, and the growth rate (convolution of the precursor concentration and the electron flux at the surface) for three different electron beam impingement positions after 0.2-s deposition time. The details of simulation methods can be found elsewhere [18], [29]. The yield of secondary electrons contributing to the precursor dissociation (deposition) reaction increases with electron beam energy, ranging 0.035–0.05 for 10 keV and 0.045–0.06 for 25 keV. Thus, the resultant reactive (secondary) electron flux also increases with electron beam energy. However, the increase in the reactive electron flux is offset by the reduction in the magnitude of the precursor surface concentration (see Fig. 7(b) and (c), first row), and the resulting growth rate (see Fig. 7(b) and (c), third row) and therefore the shape of the deposit is similar regardless of electron beam energy.

On the contrary, the location of the electron beam impingement strongly influences the shape of EBID carbon joint. Fig. 8(a) shows the cross sections of EBID carbon joint formation. When an electron beam strikes the substrate slightly off from the nanotube end, the very thin, shape-conforming carbon film is formed at the end of MWCNT contacting the multiple inner shells. This is due to the scattered secondary or backscattered electrons of an appropriate energy emerging from the surface and interacting with a diffusing hydrocarbon precursor away from the focal point of the beam striking the substrate. Focusing the electron beam at the end of the MWNT forms a very thick carbon layer in direction normal to the MWCNT end. Guided by the simulation results, we first fabricated the EBID carbon contacts with the electron beam impinging slightly apart from the ends of the MWCNT to make a thin, uniform carbon layer at the ends; this ensures the connection to the multiple shells of the tube, and the additional deposits were fabricated closer to the MWCNT ends to fully cover them with the EBID carbon joint as shown in Fig. 8(b).

3) EBID for an Ultralow-Resistance Ohmic Contact to the Multiple Shells of MWCNT: Fig. 9(a) shows a free-standing (with no contacts) open-ended MWCNT bridging the metal electrodes, which has a resistance in the order of gigaohms. This MWCNT has a diameter of ∼30 nm and the channel length of 2.2 μm, which should theoretically (3) yield ∼3.8 kΩ resistance for the outermost shell, assuming that the

nanotube is defect free. The MWCNT is expected to have 39 shells assuming the core diameter of 3 nm. Each shell can be semiconducting or metallic; however, this does not significantly influence the electrical properties of the large-diameter MWCNT since the bandgap of the tube is inversely proportional to its diameter [30]. The EBID-carbon deposits were made following the two-step procedure described in Section II-C2 to connect both ends of the targeted MWCNTs to the metal electrodes. Upon making a connection via EBID carbon deposits, the overall resistance of the MWCNT–metal interconnect dropped considerably to 300 kΩ. Further improvement of the contact resistance was achieved by thermal annealing at 350 °C (see the previous section on the EBID carbon annealing for processing details), which induced complete graphitization of the hydrogenated amorphous carbon contacts. Fig. 9(b) shows the resistance variation depending on annealing time. Initial 10-min annealing significantly reduced the resistance to 1.4 kΩ, almost three times lower than that (∼3.8 kΩ) to the outermost shell of the tube alone. This indicates that the multiple shells of the tube are connected via the EBID carbon contacts. Additional annealing for 20–25 min resulted in a further dramatic reduction of the resistance down to 116±0.1 Ω, which is the record-low value for any contact material reported to date in the literature [3], [5], [11], [16], [31], [32]. Importantly, repeated measurements showed that this low-resistance EBID contact is stable over time. We suggest that such a notable reduction in the contact resistance to the multiple shells of the MWCNT is due to formation of chemical bonds between the carbon atoms at the end of MWCNTs followed by the contraction of the EBID carbon deposit, which takes place upon transition of carbon interface from its amorphous to nanocrystalline graphitic phase [22], resulting in the mechanically and chemically improved contact between the tube and its enveloping EBID carbon.

Raman spectroscopy data in Fig. 9(c) confirm the graphitic structure of the low-resistance carbon contacts. The G-peak position and D/G ratio are 1600 cm^{-1} and 2.55, respectively, which are the characteristic of the nanocrystalline graphite. The inset in Fig. 9(c) shows a Raman map for the carbon contacts indicating that the deposits are entirely graphitic structures. Complementary TEM or XPS studies need to be performed to fully understand this phenomenon and also gain further understandings of the physical, chemical, and structural properties of these unique contact interfaces. However, experimental limitations such as sample preparations for TEM and the smaller deposit size (1 μm by 1 μm) than resolution of XPS makes it difficult to perform TEM and XPS study for the current interconnect structure.

III. Conclusion

In this study, we report on a capability of graphitized EBID carbon to produce a low-resistance Ohmic contact to multiple shells of MWCNT in the context of making high-performance electrical interconnect structure for the next-generation electronic circuits. The carbon contact shape and size effect on the MWCNT–metal interconnect performance were evaluated along with other contributing factors, such as the phase composition of the carbon joint and the MWCNT channel conductance. The low (350 °C) temperature annealing technique for graphitizing initially hydrogenated amorphous EBID carbon contacts in the presence of MWCNT, acting as a preferred phase nucleation site, was demonstrated allowing significant reduction of the contact resistance without damaging carbon nanotubes. Ultimately, a process for making an EBID carbon connection to the multiple inner shells of an MWCNT has been developed with an aid of the computer simulations, resulting in an experimentally demonstrated contact resistance down to 116 Ω. In addition to making a significant advance in reducing the carbon contact resistance, we also successfully developed the multi-MWCNT alignment/assembly technique to improve yield and scalability of the carbon nanotube positioning for the case of multi-interconnect system via a combination of the limiting-resistance dielectrophoresis and structural confinement within e-beam lithography-defined network of nanowells between the metal electrodes (see Appendix B). Resolving these major challenges may open new possibilities for interconnect applications of carbon nanotubes. Moreover, utilizing the recently developed inert-gas-assisted EBID carbon deposition technique [33], one is able to accelerate the growth rate of EBID carbon deposits by at least an order of magnitude than using conventional methods, along with improving the material purity of the EBID deposits. This provides a new exciting opportunity to overcome a low throughput limitation of the EBID process, which is a crucial concern for scalable fabrication of multi-interconnect devices.

Appendix A. Experimental Sections

A. MWCNT–Metal Interconnect Fabrication With EBID Carbon Contacts

The individual MWCNTs suspended in a DMF solution were aligned between two ∼150-nm-thick Au/Cr electrodes (fabricated on top of a SiO_2 dielectric layer with ∼1 μm thickness), using ac dielectrophoresis (DEP) with the frequency of 5 MHz and peak-to-peak voltage of 0.5–1.0 V for 1 min [12]. Quanta 200 ESEM (FEI, Inc.) operated under 0.01 Pa was employed to fabricate (via EBID) carbon contacts between an MWCNT and the metal electrodes on both ends. Residual hydrocarbons adsorbed on substrates were used as a precursor for EBID of carbon material. The EBID carbon deposits shown in Figs. 3, 5, and 9 were made by an electron beam at an energy of 25 keV and a current of ∼400 pA (spot size 5) using the Nanometer Pattern Generation System (NPGS) software.

B. Characterization

Geometric, electrical, and compositional characterization has been done according to [12], [22], [34]. Specifically,

1) AFM images shown in Fig. 1 were collected using a Dimension-3000 microscope with silicon tips of the radii between 10 and 20 nm and a spring constant of about 40 N/m. The samples were scanned at 0.5–0.7 Hz.
2) Electrical measurements were conducted by a two-terminal method in vacuum. The voltage bias was applied using SRC Model DS345 30-MHz synthesized function generator, and the current was collected using Keithley 6485 Picoammeter. The low-voltage bias ranging from 0 to 80 mV was applied to avoid Joule-heating-induced damage of the nanotube.

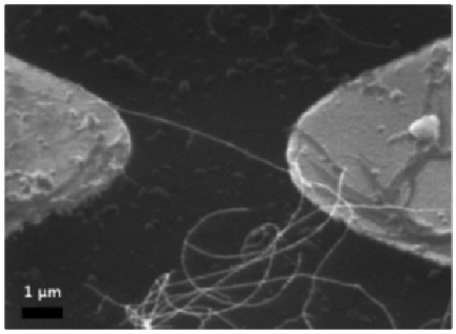

Fig. B1. SEM image of an individual MWCNT aligned using ac DEP with a 25-GΩ limiting resistor.

3) Phase composition of the EBID carbon deposits was measured using a WITec (Alpha 300R) confocal Raman microscope using Ar+ ion laser (514.5 nm) under minimum laser power (<1 mW) to avoid any laser-induced annealing. The Raman data were integrated between 1000 and 1800 cnm^{-1} to see the D- and G-band. The Lorentzian peak fitting method was applied to Raman data in order to obtain the G- and D-band peak positions and D/G peak area ratio.

Appendix B. Controlled Assembly of MWCNT With a Trench Fabricated by Electron Beam Lithography

Controlled assembly of MWCNTs into device architectures is another challenge for the application of MWCNTs to nanoelectronics. Many studies have been performed to resolve this issue [35]–[40], and the direct assembly of carbon nanotubes using DEP is found to be one of the most promising techniques due to its high controllability, low cost, and the mass-scale assembly [41]. However, there are many parameters determining an achievable yield of an individual nanotube assembly, such as MWCNT chiralities, electrode geometry, ac/dc voltage levels, ac frequency, dispersion solvent, and the geometry of carbon nanotubes [41]–[44]. The diversity of control parameters resulted in lack of consistency of an individual MWCNT assembly.

To lessen the effect of various control parameters, additional techniques were introduced by controlling electric fields generated between two metal electrodes [45], [46]. For example, the use of a large (limiting) resistor placed in a series allows for an automatic shut-off of the electric field across the metal electrodes once a carbon nanotube interconnect alignment is achieved [45]. Another technique is to use microwells fabricated by conventional photolithography, thereby creating concentrated electric fields to attract nanowires to the patterns bridging two metal electrodes [46]. Additional challenges include a highly flexible nature of carbon nanotubes with large variation in their length distribution in dispersion solution (thus, a variability of the required electric field that supports the tube alignment) and difficulty of creating metal electrodes/terminals with very sharp ends that produce better focusing of an electric field. For example, as shown in Fig. B1, we successfully aligned a single MWCNT between two electrodes with a limiting resistor of 25 GΩ, which is much larger than that of an MWCNT bridging the gap between the metal electrodes (∼1 GΩ). However, it was found that several shorter MWCNTs are also attached to the electrode side. This situation is quite typical and indicates that shorter MWCNTs can readily contaminate a designated area for assembly prior to the successful bridging of an interelectrode space by a single long tube.

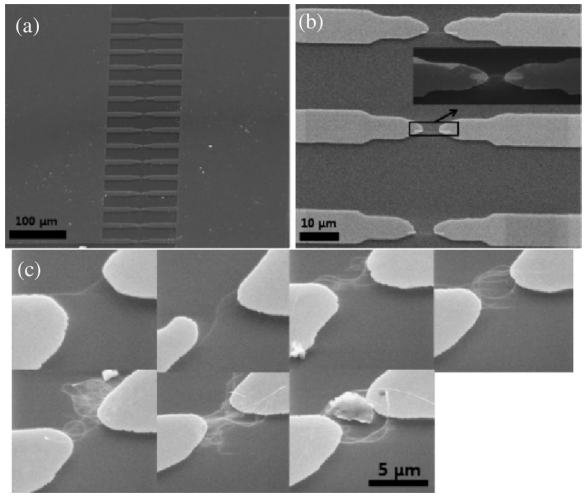

Fig. B2. (a) SEM image of 15 parallel metal pads for the CNT interconnect assembly. SEM images show the MWCNT assembly using a limiting resistor in combination with the electron beam lithography patterning. (b) 500 nm × 7 μm trenches with 120-nm depth and the inset shows MWCNTs driven to the trenches using DEP, (c) and 50% yield of MWCNT assembly after removing the photoresist.

To circumvent these challenges, we developed the concept of the limiting resistor in combination with the electron beam lithography to align MWCNTs over the multiple interconnects in an array. The test structure with 15 interconnects, as shown in Fig. B2(a), was fabricated by a conventional photolithography with Cr/SiO_2 electrodes. The positive photoresist was spin-coated with 4000 r/min for 30 s on top of the prefabricated Cr electrode. It was prebaked at 180 °C for 90 s to harden the photoresist and to evaporate the solvent. The FEI Quanta 200 SEM and "NPGS" software were used to generate the pattern. Electron beam with the spot size 3 (∼30 pA and area dose of 150 μC/cm^2) and an accelerating voltage of 25 keV was used. After developing the resist with isopropanol/ methyl-isobutyl-ketone solution, 500 nm × 7 μm trenches with 120-nm depth were obtained [see Fig. B2(b)]. MWCNTs were aligned between two electrodes using dielectrophoresis with the frequency of 5 MHz and peak-to-peak voltage of 0.5 V for 1 min. After dissolving the photoresist in acetone for 30 s, the substrate was washed with DI water and dried with N_2 gas. The inset of Fig. B2(b) shows MWCNT assembly before removing the photoresist. MWCNTs are positioned within the trench connecting two electrodes and some of them are on top of the photoresist. After removing the photoresist, only the MWCNTs in the trench remained bridging the electrodes with about 50% yield of MWCNT alignment as shown in Fig. B2(c).

Acknowledgment

The authors would like to thank O. J. Hildreth and C. P. Wong for providing MWCNT samples used in this study.

REFERENCES

[1] ITRS. (2009). *International Technology Roadmap for Semiconductors (2009 ed. Interconnect).* [Online]. Available: http://www.itrs.net

[2] J. Tersoff, "Contact resistance of carbon nanotubes," *Appl. Phys. Lett.*, vol. 74, no. 15, pp. 2122–2124, Apr. 1999.

[3] A. D. Franklin and Z. Chen, "Length scaling of carbon nanotube transistors," *Nat. Nanotechnol.*, vol. 5, pp. 858–862, Nov. 2010.

[4] R. V. Seidel, A. P. Graha, J. Kretz, B. Rajasekharan, G. S. Duesberg, M. Liebau, E. Unger, F. Kreupl, and W. Hoenlein, "Sub-20 nm short channel carbon nanotube transistors," *Nano Lett.*, vol. 5, no. 1, pp. 147–150, Nov. 2005.

[5] X. Song, X. Han, Q. Fu, J. Xu, N. Wang, and D. P. Yu, "Electrical transport measurements of the side-contacts and embedded-end-contacts of platinum leads on the same single walled carbon nanotube," *Nanotechnol.*, vol. 20, pp. 195202-1–195202-4, Nov. 2009.

[6] H. J. Li, W. G. Lu, J. J. Li, X. D. Bai, and C. Z. Gu, "Multichannel ballistic transport in multiwall carbon nanotubes," *Phys. Rev. Lett.*, vol. 95, no. 8, pp. 086601-1–086601-4, Aug. 2005.

[7] S. Frank, P. Poncharal, Z. L. Wang, and W. A. de Herr, "Carbon nanotube quantum resistors," *Sci.*, vol. 280, no. 5370, pp. 1744–1746, Jun. 1998.

[8] J. J. Palacios, A. J. Perez-Jimenez, E. SanFabian, and J. A. Verges, "First-principles phase-coherent transport in metallic nanotubes with realistic contacts," *Phys. Rev. Lett.*, vol. 90, no. 10, pp. 106801-1–106801-4, Oct. 2002.

[9] R. Pati, Y. Zhang, S. K. Nayak, and P. M. Ajayan, "Effect of H_2O adsorption on electron transport in carbon nanotube," *Appl. Phys. Lett.*, vol. 81, no. 14, pp. 2683–2640, Sep. 2002.

[10] A. Naeemi and J. D. Meindl, "Carbon nanotube interconnects," *Annu. Rev. Mater. Res.*, vol. 39, pp. 255–275, Aug. 2009.

[11] M. S. Wang, D. Golberg, and Y. Bando, "Superstrong low-resistant carbon nanotube-carbide-metal nanocontacts," *Adv. Mater.*, vol. 22, no. 47, pp. 5350–5355, Dec. 2010.

[12] K. Rykaczewski, M. R. Henry, S. K. Kim, A. G. Fedorov, D. Kulkarni, S. Singamaneni, and V. V. Tsukruk, "The effect of the geometry and material properties of a carbon joint produced by electron beam induced deposition on electrical resistance of a multiwalled carbon nanotube-to-metal contact interface," *Nanotechnol.*, vol. 21, no. 3, pp. 0352021–03520212, Jan. 2010.

[13] A. G. Fedorov and K. Rykaczewski, "Electron Beam Induced Deposition of Interface to Carbon Nanotube," U.S. Patent No. 8207058, 2012.

[14] I. Utke, P. Hoffmann, and J. Melngailis, "Gas-assisted focused electron beam and ion beam processing and fabrication," *J. Vac. Sci. Technol. B*, vol. 26, no. 4, pp. 1197–1276, Aug. 2008.

[15] S. C. Lim, J. H. Jang, D. J. Bae, G. H. Han, S. Lee, I. S. Yeo, and Y. H. Lee, "Contact resistance between metal and carbon nanotube interconnects: Effect of work function and wettability," *Appl. Phys. Lett.*, vol. 95, no. 26, pp. 264103-1–264103-3, Dec. 2009.

[16] M. Shiraishi and M. Ata, "Work function of carbon nanotubes," *Carbon*, vol. 39, no. 12, pp. 1913–1917, Oct. 2001.

[17] Y. Chai, A. Hazeghi, K. Takei, H. Y. Chen, P. C. H. Chan, A. Javey, and H. S. P. Wong, "Low-resistance electrical contact to carbon nanotubes with graphitic inter-facial layer," *IEEE Trans. Electron. Device*, vol. 59, no. 1, pp. 12–19, Jan. 2012.

[18] K. Rykaczewski, W. B. White, and A. G. Fedorov, "Analysis of electron beam induced deposition(EBID) of residual hydrocarbons in electron microscopy," *J. Appl. Phys.*, vol. 101, no. 5, pp. 054307–054319, Mar. 2007.

[19] K. Rykaczewski, A. Marshall, W. B. White, and A. G. Fedorov, "Dynamic growth of carbon nanopillars and microrings in electron beam induced dissociation of residual hydrocarbons," *Ultramicroscopy*, vol. 108, no. 9, pp. 989–992, Aug. 2008.

[20] T. H. P. Chang, M. Mankos, K. Y. Lee, and L. P. Muray, "Multiple electron-beam lithography," *Microelectron. Eng.*, vol. 57–58, pp. 117–135, Sep. 2001.

[21] H. Li, W. Y. Yin, K. Banerjee, and J. F. Mao, "Circuit modeling and performance analysis of multi-walled carbon nanotube interconnects," *IEEE Trans. Electron. Devices*, vol. 55, no. 6, pp. 1328–1337, Jun. 2008.

[22] D. D. Kulkarni, K. Rykaczewski, S. Singamaneni, S. Kim, A. G. Fedorov, and V. V. Tsukruk, "Thermally induced transformation of amorphous carbon nanostructures fabricated by electron beam induced deposition," *ACS Appl. Mater. Interfaces*, vol. 3, no. 3, pp. 710–720, Mar. 2011.

[23] T. D. Yuzvinsky, W. Mickelson, S. Aloni, G. E. Begtrup, A. Kis, and A. Zettl, "Shrinking a carbon nanotube," *Nano Lett.*, vol. 6, no. 12, pp. 2718–2722, Nov. 2006.

[24] C. A. Santini, P. M. Vereecken, A. Volodin, G. Groeseneken, S. D. Gendt, and C. V. Haesendonck, "A study of Joule heating-induced breakdown of carbon nanotube interconnects," *Nanotechnol.*, vol. 22, no. 39, pp. 395202-1–395202-9, Sep. 2011.

[25] D. Bom, R. Andrews, D. Jacques, J. Anthony, B. Chen, M. S. Meier, and J. P. Selegue, "Thermogravimetric analysis of the oxidation of the multiwalled carbon nanotubes: Evidence for the role of defect sites in carbon nanotube chemistry," *NanoLett.*, vol. 2, no. 6, pp. 615–619, May 2002.

[26] Helix Materials Solutions, Inc., 2011, www.helixmaterial.com

[27] S. Paulson, M. R. Falvo, N. Snider, A. Helser, T. Hudson, A. Seeger, R. M. Taylor, R. Superfine, and S. Washburn, "In situ resistance measurements of strained carbon nanotubes," *Appl. Phys. Lett.*, vol. 75, no. 19, pp. 2936–2938, Nov. 1999.

[28] J. F. AuBuchon, L. H. Chen, A. I. Gapin, and S. Jin, "Opening of aligned carbon nanotube ends via room-temperature sputter etching process," *J. Appl. Phys.*, vol. 97, no. 12, p. 124310, Jun. 2005.

[29] K. Rykaczewski, M. R. Henry, and A. G. Fedorov, "Electron beam induced deposition of residual hydrocarbons in the presence of a multiwall carbon nanotube," *Appl. Phys. Lett.*, vol. 95, no. 11, pp. 113112-1–113112-3, Sep. 2009.

[30] R. Saito, G. Dresselhaus, and M. Dresselhaus, *Physical Properties of Carbon Nanotubes*. London, U.K.: Imperial College Press, 1998.

[31] C. Lan, D. N. Zakharov, and R. G. Reifenberger, "Determining optimal contact length for metal/multiwalled carbon nanotube interconnect," *Appl. Phys. Lett.*, vol. 92, no. 21, pp. 213112-1–213112-3, May 2008.

[32] F. Wakaya, K. Katayama, and K. Gamo, "Contact resistance of multiwall carbon nanotubes," *Microelectron. Eng.*, vol. 67–68, pp. 853–857, Jun. 2003.

[33] M. R. Henry, S. K. Kim, and A. G. Fedorov, "Inert gas jets for growth control in electron beam induced deposition," *Appl. Phys. Lett.*, vol. 98, no. 26, pp. 263109-1–263109-3, Jun. 2011.

[34] D. D. Kulkarni, S. K. Kim, A. G. Fedorov, and V. V. Tsukruk, "Light-induced plasmon-assisted phase transformation of carbon on metal nanoparticles," *Adv. Funct. Mater.*, vol. 22, no. 10, pp. 2129–2139, May 2012.

[35] M. Burghard, G. Duesberg, G. Philip, J. Muster, and S. Roth, "Controlled adsorption of carbon nanotubes on chemically modified electrode arrays," *Adv. Mater.*, vol. 10, no. 8, pp. 584–587, May 1998.

[36] K. Lee, M. Duchamp, G. Kulik, A. Magrez, J. W. Seo, S. Jeney, A. J. Kulik, L. Forró, R. S. Sundaram, and J. Brugger, "Uniformly dispersed deposition of colloidal nanoparticles and nanowires by boiling," *Appl. Phys. Lett.*, vol. 91, no. 17, pp. 173112–173115, Oct. 2007.

[37] Y. C. Tseng, P. Xuan, A. Javey, R. Malloy, Q. Wang, J. Bokor, and H. Dai, "Monolithic integration of carbon nanotube devices with silicon MOS technology," *Nano Lett.*, vol. 4, no. 1, pp. 123–127, Dec. 2003.

[38] V. V. Tsukruk, H. Ko, and S. Peleshanko, "Nanotube surface arrays: Weaving, bending, and assembling on patterned silicon," *Phys. Rev. Lett.*, vol. 92, no. 6, pp. 065502–065502, Feb. 2004.

[39] S. G. Rao, L. Huang, W. Setyawan, and S. Hong, "Nanotube electronics: Large-scale assembly of carbon nanotubes," *Nature*, vol. 425, pp. 36–37, Sep. 2003.

[40] T. Fukuda, F. Arai, and L. Dong, "Assembly of nanodevices with carbon nanotubes through nanorobotic manipulations," *Proc. IEEE*, vol. 91, no. 11, pp. 1803–1811, Nov. 2003.

[41] M. Duchamp, K. Lee, B. Dwir, J. W. Seo, E. Kapon, L. Forró, and A. Magrez, "Controlled positioning of carbon nanotubes by dielectrophoresis: Insights into the solvent and substrate role," *ACS Nano*, vol. 4, no. 1, pp. 279–284, Jan. 2010.

[42] J. Chung, K. H. Lee, J. Lee, and R. S. Ruoff, "Toward large-scale integration of carbon nanotubes," *Langmuir*, vol. 20, no. 8, pp. 3011–3017, May 2004.

[43] R. Krupke, F. Hennrich, H. V. Löhneysen, and M. M. Kappes, "Separation of metallic from semiconducting single-walled carbon nanotubes," *Sci.*, vol. 301, no. 5631, pp. 344–347, Jul. 2003.

[44] C. W. Marquardt, S. Blatt, F. Hennrich, H. V. Löhneysen, and R. Krupke, "Probing dielectrophoretic force fields with metallic carbon nanotubes," *Appl. Phys. Lett.*, vol. 89, no. 18, pp. 183117-1–183117-3, Nov. 2006.

[45] S. Banerjee, B. White, L. Huang, B. J. Rego, S. O'Brien, and I. P. Herman, "Precise positioning of single-walled carbon nanotubes by ac dielectrophoresis," *J. Vac. Sci. Technol. B*, vol. 24, no. 6, pp. 3173–3178, Nov./Dec. 2006.

[46] T. J. Morrow, M. Li, J. Kim, T. S. Mayer, and C. D. Keating, "Programmed assembly of DNA-coated nanowire devices," *Sci.*, vol. 323, no. 5912, p. 352, Jan. 2009.

Authors' photographs and biographies not available at the time of publication.